

# Mixed Supervision Learning for Whole Slide Image Classification

Jiahui Li, Wen Chen, Xiaodi Huang, Zhiqiang Hu, Qi Duan, Hongsheng Li, Dimitris N. Metaxas, Shaoting Zhang

**Abstract**—Weak supervision learning on classification labels has demonstrated high performance in various tasks. When a few pixel-level fine annotations are also affordable, it is natural to leverage both of the pixel-level (e.g., segmentation) and image level (e.g., classification) annotation to further improve the performance. In computational pathology, however, such weak or mixed supervision learning is still a challenging task, since the high resolution of whole slide images makes it unattainable to perform end-to-end training of classification models. An alternative approach is to analyze such data by patch-based model training, i.e., using self-supervised learning to generate pixel-level pseudo labels for patches. However, such methods usually have model drifting issues, i.e., hard to converge, because the noise accumulates during the self-training process. To handle those problems, we propose a mixed supervision learning framework for super high-resolution images to effectively utilize their various labels (e.g., sufficient image-level coarse annotations and a few pixel-level fine labels). During the patch training stage, this framework can make use of coarse image-level labels to refine self-supervised learning and generate high-quality pixel-level pseudo labels. A comprehensive strategy is proposed to suppress pixel-level false positives and false negatives. Three real-world datasets with very large number of images (i.e., more than 10,000 whole slide images) and various types of labels are used to evaluate the effectiveness of mixed supervision learning. We reduced the false positive rate by around one third compared to state of the art while retaining 100% sensitivity, in the task of image-level classification.

**Index Terms**—Computational pathology, Mixed & Weak supervision learning, Whole slide image, High resolution images

## I. INTRODUCTION

Mixed supervision learning on various levels of annotations has shown its effectiveness in various machine learning applications [1]–[3]. However, in the context of computational pathology, this is still a challenging problem, as the high-resolution of whole slide images makes it unattainable to conduct end-to-end training of deep learning models using

existing weak or mixed supervision learning methods [1], [2], [4]–[12]. As the size of pathological whole slide images is around  $100,000 \times 100,000$  pixels, the discriminative regions usually only occupy a small portion of the image. Such high-resolution images with classification labels and small discriminative areas are thus infeasible to be end-to-end trained with limited GPU memory. Patch-based training is the compromising choice to analyze such data. Self-supervised learning can be used to generate pixel-level pseudo labels for patches [13], [14]. Then the difficulty comes to how to use image-level labels to refine the quality of pseudo labels on patches, without training on the whole image, while still utilizing pixel-level fine-grained labels.

To address the aforementioned issues, a novel mixed supervision learning framework is proposed for the classification of whole slide images, i.e., to distinguish positive or negative. As we can only train deep learning models on patches, a well-designed strategy is designed to modify pixel-level pseudo labels on patches, according to image-level labels. Specifically, a positive image is guaranteed to contain at least one true positive patch, while negative images are composed entirely of negative pixels. In addition, pixel-level errors, i.e., false negatives and false positives, are gathered during pseudo labels generation. We perform re-weighting on pixel-level pseudo labels of patches from positive images, converting false negatives to true positives and false positives. Hard negative patches are mined from negative images with a higher sampling ratio to train models, to further modify false positives to true negatives. The reason is that noise tolerant deep learning model can discriminate a pattern as negative if it is mostly labeled as negative during training. As for the few pixel-level annotations, we use them to initialize pre-trained models and to mix a constant ratio in each training batch with pixel-level pseudo labels to regularize training. With such strategy, without end-to-end training, we can fully utilize image-level labels, pixel-level fine-grained labels and pseudo labels in unlabeled areas.

Existing datasets are either with large data volume but weak annotations [14], or with fine annotations but small data volume [15]. To evaluate the effectiveness of our mixed supervision learning, we conducted extensive experiments on three large real-world datasets of different modality, with full image-level labels and a few pixel-level annotations. The first one is Hematoxylin and eosin (H&E) stained gastric biopsy pathology whole-slide images, containing 200 pixel-level fine-grained labeled patches, 1,084 positive and 9,810

Manuscript received July 1, 2020. This study has been financially supported by fund of STCSM(19511121400), also supported by SenseTime Research. (Corresponding author: Shaoting Zhang.)

Jiahui Li, Wen Chen, Xiaodi Huang, Zhiqiang Hu, Qi Duan, Shaoting Zhang are with SenseTime Research (e-mail: zhangshaoting@sensetime.com).

Hongsheng Li is with The Chinese University of Hong Kong  
Dimitris N. Metaxas is with Rutgers University

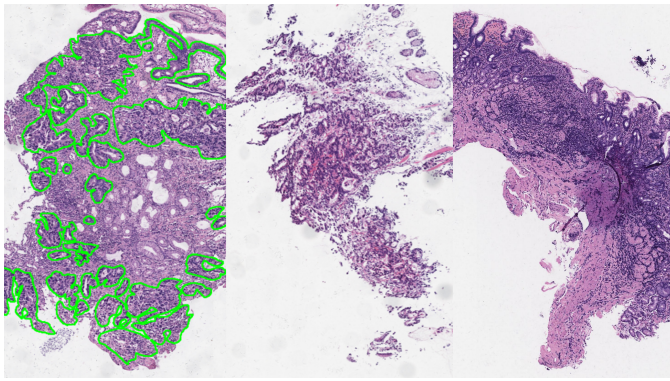


Fig. 1. Illustration of mixed supervision data, containing 2 types of label. The first expensive and rare type is pixel-level fine-grained labels, contoured by green lines. The second type is image-level labeled images. The rest two images are image-level positive and negative.

negative image-level whole slide images, 10,894 in total. Pixel-level fine-grained labels are annotated by multiple pathologists while image-level labels are extracted from clinical reports. The second dataset is whole slide images from cervical cytology, containing data from 2 medical centers, with 8,494 bounding box-level labeled cells, 317 positive and 545 negative image-level labeled whole slide images, 862 in total. Cells with positive labels are responsible for further diagnosis. The third dataset is Camelyon17 [16], which is a public challenge. There are 500 whole slide images for test, 500 for training with image-level annotations. Among 500 image-level labeled whole slide images, 50 were provided with pixel-level labels. Camelyon16 also released 110 images with pixel-level labels permitted to use. Evaluation metrics is the kappa score of 5 classes whole slide image classification.

The main contribution of our mixed supervision learning framework is to utilize both the limited amount of pixel-level annotations and the large number of image-level labels. Without end-to-end image-level training, image-level labels are used to refine pseudo labels on the entire training dataset, with well-designed strategy to control false positives and false negatives. We have evaluated the framework on three large pathology whole slide images datasets of histopathology and cytology, which are among the largest datasets in computational pathology literature. According to experiment results, for the histopathology dataset, mixed supervision learning shows specificity 8.92% better than image-level training and 5.2% better than pixel-level training, while retaining 100% sensitivity. For the cytopathology dataset, mixed supervision learning achieves specificity 14% better than pixel-level training on the unlabeled center source, while image-level training fails on this dataset for tiny ratio of positive cells. For Camelyon17, we achieve kappa score 92.43%, 4th in leaderboard. Outperform the 90.90%, 5th with 1.53%, whose code we use as pixel-level baseline in the previous two experiments.

## II. RELATED WORK

### A. Mixed supervision learning

In many medical image analysis tasks, it is common to have various types of labels available, e.g., a large number of

clinical reports and a small group of segmentation annotations shown in Fig. 1, so called mixed supervision. However, this observation has not been well investigated before. Instead, focus was given to semi and weak supervision learning [15], [17]–[20], either rely on pixel-level or image-level annotations, combined with unlabeled images. The most relevant research to our framework is from [1]–[3], in which the same model with both segmentation and classification output branch is jointly trained on two types of data. Our framework is different from theirs because the end-to-end classification training with entire image input is difficult due to massive size of whole slide images. Instead, only patches are involved in our total pipeline, image-level labels are not directly related to loss calculation.

In the context of self-supervised learning methods, most of the existing approaches [21] correctly generated pixel-level pseudo labels, refined pseudo labels by complex prior knowledge, for examples high-quality initial models [20], multi-models consistency [15], [22], [23], video frames sequence consistency [24], auto encoder [25], discriminator to distinguish annotations and predicted mask [26], interactive annotation [27]–[30], and unsupervised representation learning followed by fast tuning for specific tasks [31]–[36]. For medical image analysis, coarse image-level annotations can be obtained efficiently from numerous clinical reports, while pixel-level annotations must be manually annotated. Thus, in our task, image-level label is a proper coarse refinement for pixel-level pseudo labels.

### B. Computational Pathology: methods and datasets

There exists lots of works related to computational pathology besides whole slide image classification, including nuclei and gland segmentation [37]–[40], genetic analysis [41]–[45], immunohistochemistry [46]–[48], clinical relation [49] and so on. Usually the size of one whole slide image is around  $100,000 \times 100,000$  pixels, which is infeasible to run directly on GPU. Therefore, most of previous methods process images in a two-stage manner [13], [14], [50]–[54]. In the first stage, most existing studies partition whole slide images into patches and execute the analysis on each patch separately. During the second stage, a whole slide image classifier is trained on the selected patches from the first stage. Campanella et al. [14] proposed a weak supervision learning framework on pathology whole slide images with image-level labels. Without using pixel-level annotations, the top responsible patches are searched for image-level labels. A large dataset of image-level labeled 44,732 slides are evaluated. The released source code is employed as the image-level comparison baseline in our paper. Another large dataset comes from [51]. Their grading and segmentation of prostate pathology was developed by 8,313 whole slide images in total, showing similar grading performance with pathologists. This work is done in full pixel-level annotated manner. The Cancer Genome Atlas (TCGA) [55] is also a well-known data repository, containing more than two petabytes of genomic data of multi dimensional maps of prime genomic deviation in 33 categories of cancer. In summary, for computational pathology, a dataset shall contain

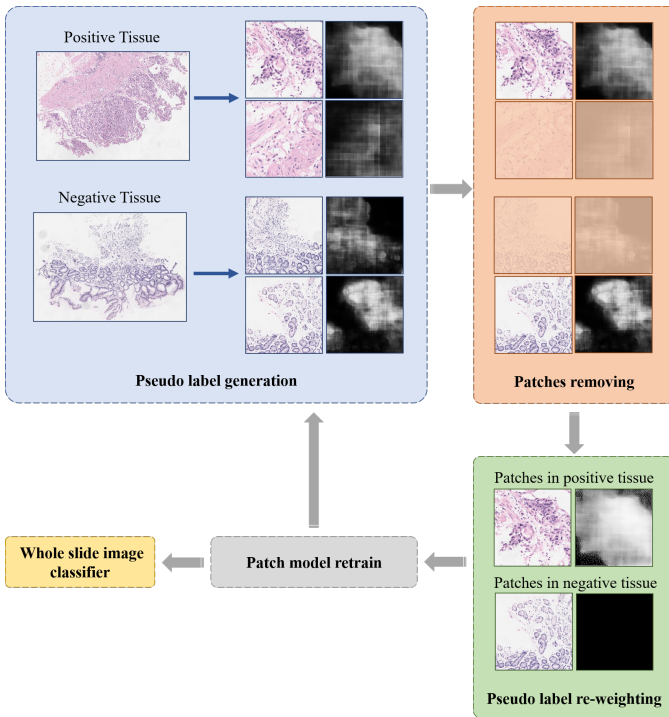


Fig. 2. The overall pipeline of our mixed supervision learning for pathology whole slide image. The image-level label guided pixel-level pseudo label generation is iterated in this manner. The gray scale map is the predicted probability map of patch model.

large numbers of whole slide images with clinical reports to verify effectiveness of the proposed algorithms, and evaluation metrics are mostly related to image-level classification.

Recently, several works enable the possibility to train gigapixels whole slide image classification in an end-to-end manner. For example, the method proposed by Takahama et al. [56] directly communicated the gradients from image classifier to patches encoder by cache tricks. Promising accuracy can be achieved with careful implementation and parameter tuning. The second one is the graph convolution network [57], which is possible to compress the huge whole slide image into nuclei graph representation. The premise of nuclei graph net is to form the graph by a high-performance nuclei instance segmentation model, which organizes position and appearance feature of nuclei. This process contains two stages, i.e., the nuclei instance segmentation and the graph convolution model. End-to-end training whole slide image classifier requires much more programming to reduce GPU memory usage, but does not show a higher level of accuracy than two-stage manner. We choose to use the two-stage strategy, since an end-to-end whole slide classifier has a high risk of missing positive slides which contain tiny positive regions. Small target classification has been a difficult task for a long time, and the two-stage pipeline allows us to discard most negative regions, and feed the most suspicious patches to the image classifier.

### III. MIXED SUPERVISION LEARNING

Due to the extreme large size of the whole slide images (e.g., larger than  $10,000 \times 10,000$ ), it is infeasible to use conventional weak supervision approaches. The mixed supervision

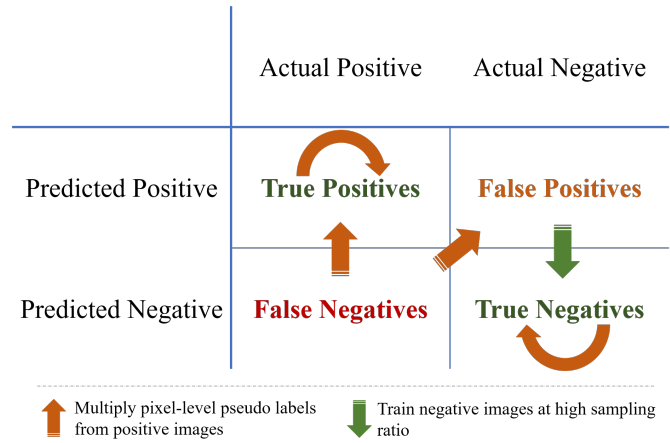


Fig. 3. Strategy to control false negatives and false positives.

learning aims to use image-level labels to refine pixel-level pseudo labels on patches, without the entire huge image input. Our algorithm framework is shown in Fig. 2 and Algorithm. 1, which involves two stages: the patch segmentation stage, and the whole slide image classification stage.

During stage 1, patch segmentation stage, a clinically effective system can tolerate false positives for further recheck by pathologists, while false negatives are vital faults for patients. Thus, we need to locate the positive patterns in positive images as much as possible, while precluding more negative images. Our goal is to maintain 100% sensitivity and pursue higher specificity to reduce workloads. With this consideration, comparing positive images and negative images, patterns that only exist in positive images shall all be suspicious and at least one patch is responsible for image-level positive diagnosis. Also, negative patterns that exist in negative images can certainly be regarded as true negative patterns, and positive predictions in negative images can be regarded as hard negative patches. Meanwhile, collecting negative images is much easier than positive images. With sufficient suppression of various hard negative patches, a positive growing tendency is given to patterns in positive images. Only the confidence of those true positive patterns is able to gradually grow up and reach 1.0 eventually. Those noisy false positives introduced by growing tendency are suppressed by various hard negative patches and higher sampling ratio during deep learning model training. As for pixel-level fine-grained labels  $y_p$ , the best performance can be attained if all pixel-level fine-grained labels can be performed for all positive images. However, the limited computational resource can just afford a portion, whose quantity is significantly smaller than the image-level labels. To involve pixel-level fine-grained labels  $y_p$  into training, it is used to initialize a pre-trained model  $\theta_1$ , to minimize false positives and false negatives at the beginning. Then, it consists of a large ratio in each training batch.

To achieve those shown in Fig. 3 and Fig. 2, we separate large size of whole slide images into patches, then develop an *Expectation-Maximization (EM)*-like method to make full use of three types of annotation: image-level labels  $y_i$ , pixel-level fine-grained labels  $y_p$  and pixel-level pseudo labels  $\hat{y}_p$ .

In the E-step, pixel-level pseudo labels  $\hat{y}_p$  are firstly created



**Algorithm 1:** Pipeline of mixed supervision learning.**Data:**

$y_p$ : pixel-level fine-grained label from pathologists.  
 $\hat{y}_p, y_{p+}, y_{p-}$ : pixel-level pseudo label, from positive and negative images, created by models and image-level labels guided re-weighting.  
 $y_i$ : image-level label from clinical reports.  
 $\theta_1$ : patch segmentation model initially trained by  $y_p$ , outputs the probability that each pixel of input patch is positive.  
 $\theta_2$ : whole slide image classifier, outputs the probability that input whole slide image is positive.  
 $I$ : high resolution whole slide image.  
 $x$ : image patches.  
 $T$ : patch removing threshold.  
 $V$ : re-weighting constant.  
 $R$ : sampling ratio of  $y_p, y_{p+}$  and  $y_{p-}$ .  
 $K$ : select top  $K$  patches as input to train whole slide image classifier.

**while** the model do not converge **do**

**Stage 1: patch segmentation ;**

**E-step:**  $\hat{y}_p \leftarrow P(y_p|x, \theta_1)$  ;

Remove those patch  $x$  whose maximum pixel-level  $\hat{y}_p$  in this patch is less than  $T$  ;

**if**  $y_i == 1$  **then**

$y_{p+} \leftarrow \hat{y}_p \times V$  (pseudo labels);  
 $y_{p+} \leftarrow 1.0$  if  $\hat{y}_{p+} > 1.0$  (clip within 1.0, to remain true positive);  
 $y_{p+} \leftarrow 0.0$  if  $\hat{y}_{p+} < 0.01$  (clip to 0.0 if lower than 0.01, to remain true negative which was slightly scaled up by  $V$ );

**else**

$y_{p-} \leftarrow 0$  (hard negative labels);

**M-step:** Retrain patch segmentation model  $\theta_1$  at proper sampling ratio of  $R$  in each training batch, and by pixel-level soft label cross entropy loss =  $-\frac{1}{N} \sum_N \sum_{y=y_p \cup y_{p+} \cup y_{p-}} y \times \log P(y_p|x, \theta_1) + (1.0 - y) \times \log(1.0 - P(y_p|x, \theta_1))$  ;

**Stage 2: whole slide image classification ;**

Select top  $K$  patches for each whole slide image according to pixel-level maximum  $P(y_p|x, \theta_1)$ ;

$P(y_i|I, \theta_2) = \frac{1}{K} \sum_K P(y_i|x, \theta_2)$

Train classification model  $\theta_2$  by Loss =  $-\frac{1}{N} \sum_N y_i \times \log P(y_i|I, \theta_2) + (1.0 - y_i) \times \log(1.0 - P(y_i|I, \theta_2))$

**Convergence criteria:** For each round of stage1, perform stage2 training. Select the round whose stage2 training loss is the lowest, which means the top  $K$  patches selected in that round by stage1 is the optimal to fit image-level annotations.

number of training patches. Provided with image-level labels, we obtain hard negative patches  $y_{p-}$  from negative images and noisy pseudo labeled positive patches from positive images. Then, the weight  $V$  ( $V > 1$ ) is multiplied on noisy pseudo labels in positive patches and clipped with in 1.0, assigning them as  $y_{p+}$ , which transforms false negatives to true positives and false positives, while keeping true positives as the same. Those pseudo labels less than 0.01 are clipped to zero to remain true negatives. As confidence of true negative pixels is close to zero, which is less than 0.01 even scaled up by  $V$ .

In the M-step, patch segmentation model is then trained on a sampling ratio of pixel-level fine-grained labels  $y_p$ , pseudo labeled positive patches  $y_{p+}$  and hard negative patches  $y_{p-}$ . For sampling ratio of  $y_p, y_{p+}$  and  $y_{p-}$  in each training batch, hard negative patches  $y_{p-}$  shall be much more than pseudo labeled positive patches  $y_{p+}$  so that if one pattern is both labeled as negative in hard negative patches and positive in pseudo labeled patches, model can still regard such pattern as negative for much higher sampling ratio, which transforms false positives to true negatives. Only those patterns not suppressed by negative patches are possible to be eventually discriminated as positive by models. Such procedure is iterated for several rounds until converge. The pixel-level soft-label cross entropy is used as the loss function in patch segmentation stage, to deal with both soft pseudo and fine-grained labels.

In Stage 2, whole slide image classification, for each whole slide image, top  $K$  patches with maximum pixel-level probability are the input to image classifier  $\theta_2$ . Average probability is the final image-level confidence to calculate loss with image-level labels. Stage2 training also decides the convergence criteria. We perform stage2 training for each round of stage1 and select that round whose stage2 training loss is the lowest. That means the top  $K$  patches selected in this round by stage1 is the optimal to fit image-level annotations in stage2.

## IV. EXPERIMENTS

In section A we presented two comparison baselines for our mixed supervision learning. The practical impact of varying those hyper-parameters will be discussed in Section B. Following the evaluation protocol stated above, we presented results on three real-world datasets in terms of performance in section C,D,E. We also discuss convergence criterion and the necessary size of two types of annotations by ablation study in F.

### A. Experimental setting

To evaluate the effectiveness of mixed supervision learning, we designed three experiments using different supervision for comparison: **image-level**, **pixel-level** and **mixed**. **Image-level** experiment is conducted based on the source code from Campanella et al [14], whose multi-instance learning method relies only on image-level labels and searches top  $K$  responsible patches for image-level labels. Without pixel-level fine-grained labels to initialize, patch model is an ImageNet pre-trained classification model. Patch classification model predicts every patch's confidence in an image to be positive, then top  $K$  patches are further trained by image-level labels.

from segmentation confidence map of patches from both positive and negative images. We remove all the patches from both positive and negative images whose maximum pixel-level positive confidence is less than a threshold  $T$ , to reduce the



It is  $K = 1$  in the released code [14]. **Pixel-level** experiment is conducted based on source code of Mahendra Khened et al [53]. This generalized pathology processing framework is the 5th in Camelyon17 Challenge<sup>1</sup> [16], 4th in DigestPath2019<sup>2</sup> [15] and 3rd in PAIP challenge<sup>3</sup>. It uses all of existing pixel-level fine-grained labels to train patch segmentation model and image-level labels to train whole slide image classification model, without extracting hidden pixel-level pseudo labels. **Mixed** experiment makes use of image-level labels, pixel-level fine-grained labels, and pseudo labels which are generated from the aforementioned two. For Camelyon17 [16], stage2 is replaced with random forest, whose input is morphological features of downsampled segmentation result from stage1.

The evaluation metrics include sensitivity, specificity, receiver operating characteristic (ROC) curve and area under the ROC Curve (AUC). The aim is to achieve higher specificity while retaining 100% sensitivity. For Camelyon17 [16], evaluation metrics is multi class kappa score for whole slide images classification, refer to pN0, pN0(+), pN1mi, pN1, pN2.

### B. Implementation details

**Hyper-parameters:** We stop stage1 at round3 because of the minimum stage2 training loss among round1 to round4. Re-weighting constant is  $V = 4.0$  for all the experiments. This value only influences the training time, e.g., the lower  $V$  is, the longer time it takes.  $V$  bigger than 4.0 shows no significant improvement in speed. The pixel-wise maximum confidence patch selection threshold  $T$  is 0.4. Higher threshold  $T$  can exclude some positive whole slide images when comes to round1, and thus degrades sensitivity. Lower threshold  $T$  introduces too many patches during training, leading to longer convergence time but nearly the same final performance. Patch size for both patch segmentation and whole slide image classification is set as  $H = 512$ ,  $W = 512$ , overlapped 128.  $K$  is set as 16 for the classification of top  $K$  patches. During patch segmentation model training,  $R$ , sampling ratio of pixel-level fine-grained labels  $y_p$ , pseudo labels  $y_{p+}$  and hard negative patches  $y_{p-}$  is 2:1:7, to allow hard negative patches to dominate wrong patterns in noisy positive pseudo labels and keep pixel-level fine-grained labels participating in training procedure. Sampling ratio  $R = 2:1:7$  would ensure the noisy labels ratio at most reach 10%, for the worse case when all the pseudo labels are incorrect. Deep learning model is capable to tolerate such noisy ratio according to [58], with little performance drop. For multi-round iteration, patch model initializes the weights from previous round, not from scratch. For whole slide image classifier, the sampling ratio of positive and negative images is equal. During training each round, patch model is trained 30 epochs while whole slide image classifier is trained 15 epochs.

**Base environment:** A computing cluster is used during the experiments, with 11 nodes and 8 Nvidia 1080ti GPUs for each node. Deep learning algorithms are implemented with Pytorch1.0 [59] along with Openslide3.4.1 [60]. Otsu’s

<sup>1</sup><https://camelyon17.grand-challenge.org/evaluation/challenge/leaderboard/>

<sup>2</sup><https://digestpath2019.grand-challenge.org>

<sup>3</sup><https://paip2019.grand-challenge.org/Leaderboard>

TABLE I  
DATA DISTRIBUTION AND TRAIN/TEST SEPARATION OF GASTRIC CANCER DATASET

Distribution	Pixel-level Train set	Images Train set	Images Test set	Total Images	Total Patients
Positive	200 big patches 113 images related	585	499	1,084	724
Negative	0	4,096	5,714	9,810	5941
Total	200 big patches	4,681	6,213	10,894	6,665

TABLE II  
STATISTICS RESULTS OF GASTRIC CANCER DATASET

Metrics	Mixed	Pixel-level [53]	Image-level [14]
Sensitivity	1.0000	1.0000	1.0000
Specificity	<b>0.8932</b>	0.8412	0.8040
AUC	<b>0.9906</b>	0.9848	0.9705
Threshold	0.1000	0.0041	0.0012

[61] thresholding technique is used to extract tissue regions. DLA34up and DLA34 [62] are patch segmentation and whole slide image classification models  $\theta_1, \theta_2$ .

### C. Evaluation on the gastric cancer dataset

1) **Dataset:** The first dataset of gastric cancer microscopic tissue is collected from four hospitals and 10,894 whole slide images in total, which is gathered from 6,665 patients. All the slides are automatically scanned by digital pathology scanner Leica Aperio AT2 at 20X magnification (0.50 $\mu$ m/pixel). The pixel-level fine-grained labeled big patches are on average 4,000 pixels in height and width, manually annotated by at least two board-certified pathologists. Whole slide images are of around 100,000 pixels height and width. Data distribution of pixel-level fine-grained labeled patches, positive and negative whole slides, train/test separation are shown in Tab. I, this ratio 1:9 of positive and negative is approximately the same distribution of clinical daily works. The image-level annotation is either ‘Positive’, which refers to low-grade intraepithelial neoplasia, high-grade intraepithelial neoplasia, adenocarcinoma, signet ring cell carcinoma, and poorly cohesive carcinoma, or ‘Negative’, including chronic atrophic gastritis, chronic non-atrophic gastritis, intestinal metaplasia, gastric polyps, gastric mucosal erosion, etc.

2) **Results:** Public code of Campanella et al. [14] is the baseline for using image-level annotations. This code can produce patch-level classification probability, instead of pixel-level, shown as the blocks in second row of Fig. 5. Statistically, their multi-instance learning on our data achieve 80.40% specificity while retaining 100% sensitivity at binary threshold  $P = 0.0012$ . At the same time, our mixed supervision framework can achieve 89.32% specificity with 100% sensitivity at threshold  $P = 0.1000$ , 8.92% far more than image-level annotation. These are summarized in Fig. 4. The mixed supervision learning could eventually reach 0.9049 specificity at threshold = 0.1421, while the rest two baselines have to use extremely low threshold for 100% sensitivity, due to less supervision information.

The reason for this phenomenon is that with image-level

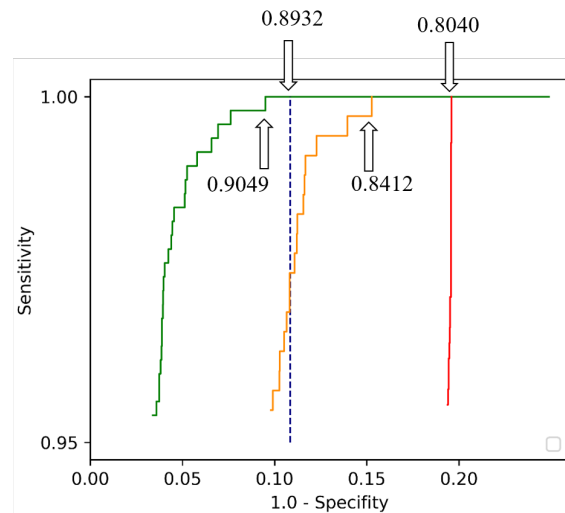
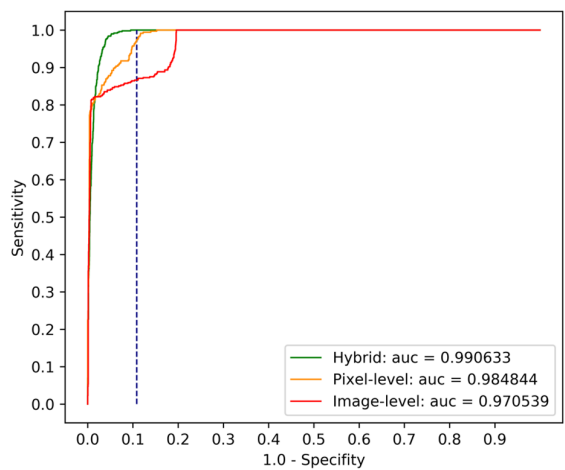


Fig. 4. ROC curve detail of the three setting. In fact mixed supervision learning can finally achieve specificity 0.9049 at probability threshold 0.1421

labels only, Campanella et al [14] searches the minimum representative patches responsible for image-level labels, without covering the most positive regions, shown in Fig. 5. At the same time, our mixed supervision learning framework is trained on most of positive patches in each positive whole slide image. More positive training samples establish finer-scales of boundary between positive and negative patches, leading to higher specificity and area under curve.

Based on code of Mahendra Khened et al [53], 200 pixel-level fine-grained labeled big patches are used to train the initial patch segmentation model. Then, top patches are selected for whole slide images classifier training, without image-level labels guided pixel-level pseudo labels generation. This configuration achieves 84.12% specificity, 5.2% lower than mixed supervision learning, indicating the proposed mixed supervision learning is better than simple backbones sharing manner.

Visually shown in Fig. 5, pixel-level training is sensitive to positive boundary but miss several positive regions, which is then covered by mixed supervision learning. We prefer higher positive coverage, which is much more important than positive boundary.

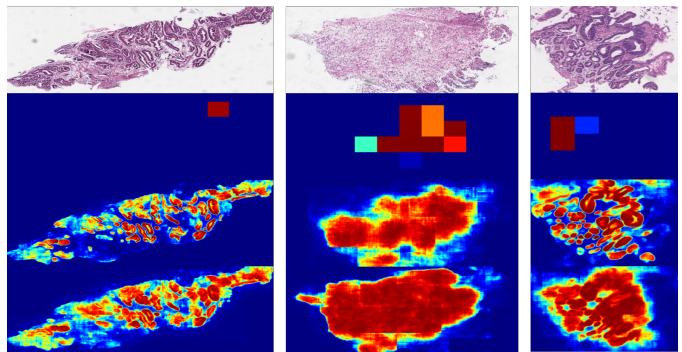


Fig. 5. Four rows are original images, heatmaps of image-level, pixel-level and mixed supervision prediction. Image-level training only locates the smallest number of patches enough for image-level positive prediction. Mixed supervision learning covers more tumor region than pixel-level and image-level training, although less sensitive to tumor boundary compared to pixel-level.

TABLE III

DATA DISTRIBUTION OF CERVICAL CYTOLOGY DATASET. NUMBER OF PATIENTS IS THE SAME AS IMAGES.

	Pixel-level Center B	Images Center A	Images Center B	Total images	Total patients
Positive	8,494 cells	238	79	317	317
Negative	0	441	104	545	545
Total	8,494 cells	679	183	862	862

#### D. Evaluation on the cervical cytology dataset

1) *Dataset*: In cervical cytology dataset, thousands of sparse cells are flattened for pathologists to find positive cells responsible for diagnosis, which has been a time-consuming and tedious procedure. This dataset is collected from 2 data centers, related to 862 patients in total, whose major differences are the operation styles of two groups pathologists. Distribution is detailed stated in Tab. III. Pixel-level fine-grained labels are only performed on center B, the minor one. The collected dataset covers most of abnormal cells required by The Bethesda System (TBS), including LSIL, HSIL, ASC-US, ASC-H and so on. We define all of them as ‘Positive cells’.

For evaluation, 2-fold cross validation of binary image-level classification is performed to reveal performance on entire dataset, in each fold each center is separated half for training and test. Hyper-parameters, scanners and training environment are the same as gastric cancer dataset.

2) *Results*: The same as the gastric cancer dataset, models are trained on image-level [14], pixel-level [53] and mixed setting. Image-level [14] experiment on cervical cytology failed to converge for extremely tiny positive cells ratio. In pixel-level training [53], initial labels are provided on center B. Specificity 81% is achieved on center B but drops to 72% on center A due to domain gap. To solve domain gap problem the direct solution is to train data from that source, even on noisy pseudo labeled data. This is exactly what we do in mixed supervision learning. By the refinement from image-level labels, we correctly extract pixel-level annotations in both of pixel-level unlabeled center A and unlabeled regions in center B. On pixel-level unlabeled center A, while retaining

TABLE IV

MIXED SUPERVISION LEARNING ON CERVICAL CYTOLOGY DATASET			
Performance	Image-level [14] Center A	Pixel-level [53] Center A	Mixed Center A
Sensitivity	65%	100%	100%
Specificity	67%	72%	86%
Performance	Image-level [14] Center B	Pixel-level [53] Center B	Mixed Center B
Sensitivity	67%	100%	100%
Specificity	69%	81%	87%

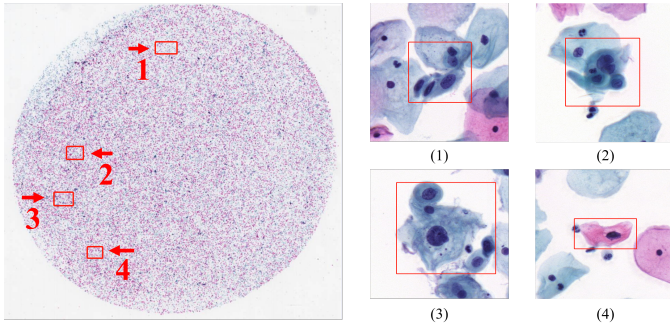


Fig. 6. Top four possible positive cells found by mixed supervision learning, visualized by bounding box of segmentation results. Our mixed supervision learning can precisely direct pathologists to suspicious cells in huge whole slide images.

100% sensitivity, specificity is improved from 72% to 86%, a bonus of 14%. For center B, 6% more specificity is also introduced by mixed supervision learning.

### E. Evaluation on the Camelyon17

Camelyon17 is a public whole slide images classification challenge, requiring participants to assign each whole slide image with one of pN0, pN0(i+), pN1mi, pN1, pN2, ascending related to the size of tumor region. This challenge releases 500 images for test, 450 training images with image-level labels, 50 training images with both of pixel-level and image-level annotations. Data from Camelyon16 is also allowed for training, which contains 110 positive images with pixel-level labels and 160 negative images. Thus this challenge is a five classes classification problem, strongly related to the region of binary pixel segmentation. In this challenge we replace stage2 by random forest classifier with morphological features of the whole slide image segmentation maps. According to leaderboard<sup>4</sup> of Camelyon17 [16], more than 100 valid scores have taken places from various famous institutions. During previous experiments we establish mixed, pixel-level and image-level setting. In this challenge, whose number of training whole slide images is less than 1000, image-level procedure achieves kappa score 74.05%, 71st. Such unsatisfactory result makes us believe thousands of training whole slide images is necessary for image-level pipeline to converge. Pixel-level [53] setting reaches 90.90%, 5th in leaderboard, whose generalization has been validated in various challenges. Our mixed supervision

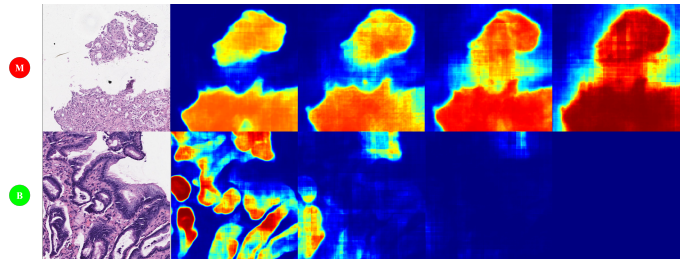


Fig. 7. Visualization of pseudo labels of initialization, round1, round2 and round3. For positive images in first row, by image-level refinement, positive confidence grows at the sacrifice of coarse boundary and limited false positives. For negative images, pixel-level labels finally reach pure zero. Confidence of true positives are still higher than false positives, which will not change inputs to whole slide image classifier.

learning is the 92.43%, 4th, which is 1.53% more than pixel-level baseline. The CNN architectures of pixel-level baseline is the ensemble of DeeplabV3+, DenseNet121 and Inception-ResnetV2, which is much deeper and complex than our Deep Layer Aggregation 34 layers. However, the worse score of pixel-level indicates that data utility is the key for higher performance, rather than complexity or depth of CNN architectures. The 92.73%, 3rd is quite similar to ours. The higher score of the 95.70%, 1st and 93.86%, 2nd are the results of sophisticated online hard mining, multi-scale ensembles strategy and careful hyper parameters tuning. Certainly these are all the promise of higher scores but beyond the scope of this paper.

### F. Ablation Study

1) *Heatmap visualization across each round*: Since the patch segmentation stage is trained in an iterative manner, an intrinsic problem is to check whether pixel-level pseudo labels behave as expected in each round. For negative images, pure zero is eventually expected. For positive images, with image-level supervision exact positive boundary is hard to achieve, and more positive region shall be covered by coarse boundary, as shown in Fig. 7. For positive image in first row, the first heatmap is the prediction from pixel-level models. It produces exact boundary of these two tumors with a relative low confidence, due to domain gap between annotated patches and new positive images. The next three heatmaps come from round1 to round3. Due to image-level refinement only, pixel-level confidence gradually grows and covers all the tumor while including a few false positives nearby tumor. Relative the true tumor confidence is still higher than false positives, which will not change top K inputs to whole slide classifier. While we train hard negative samples from negative images at high sampling ratio, false positives in positive images are well restricted just nearby tumor regions. For negative image in second row, pseudo labels gradually decrease to pure zero.

2) *Size of pixel-level fine-grained labels and training whole slide images*: The size of pixel-level fine-grained labels shall be as large as possible within acceptable annotation cost. While collecting whole slide images with classification reports could be cheap. In this part two experiments are conducted to check the influence of data size, fix to round3: Full size

<sup>4</sup><https://camelyon17.grand-challenge.org/evaluation/challenge/leaderboard/>



TABLE V

UNDER REQUIREMENT OF 100% SENSITIVITY, PERFORMANCE CHANGES OF DIFFERENT TRAINING WHOLE SLIDES NUMBER AND PIXEL-LEVEL FINE-GRAINED LABELS. POSITIVE/NEGATIVE WHOLE SLIDE NUMBER IS PRECISELY STATED.

Whole slides number	585/4,096	348/2,048	231/1,019	174/510
Pixel-level labels size	200	200	200	200
Specificity	89.32%	89.01%	87.94%	79.15%
Whole slides number	585/4,096	585/4,096	585/4,096	585/4,096
Pixel-level labels size	200	100	50	25
Specificity	89.32%	88.09%	84.77%	71.27%

of pixel-level fine-grained labels and changes of training slides, full size of training slides and changes of pixel-level fine-grained labels. As shown in Tab. V, as the number of whole slides image or pixel-level fine-grained labels decreases specificity gradually decreases. Sudden drop happens in both experiments if one type of training data decreases to 1/8 of the total number and provides worse performance than Image-level multi-instance learning [14]. This phenomenon tells us that certain minimum necessary numbers exist for both types of training data, otherwise may mislead training procedure, especially the pixel-level fine-grained labels. The performance degradation of limited pixel-level fine-grained labels is much more than limited training whole slide images. Thus the minimum required number of pixel-level fine-grained labels is the number that enables mixed supervision learning to surpass pure image-level training, which is between 25 and 50 patches in our data.

## V. CONCLUSIONS

In this paper, we propose a novel mixed supervision framework for whole slide image classification. The main contribution is to use image-level labels for self-supervised learning to generate high-quality pixel-level pseudo labels on patches, without using whole images for end-to-end classification training. Pixel-level false negatives are prevented by re-weighting on pseudo labels of selected patches from positive images. False positives error is suppressed by high training sampling ratio of hard negative patches from negative images. Using this framework and a few pixel-level fine-grained labeled data, one can utilize large amount of image-level labeled whole slide images, train models in segmentation manner, and get much higher performance compared to using single format of annotation only, or just the existing labels. Comprehensive experiments are done on three large mixed annotated datasets, demonstrating the high effectiveness and generalization of our mixed supervision learning.

## REFERENCES

[1] P. Mlynarski, H. Delingette, A. Criminisi, and N. Ayache, "Deep learning with mixed supervision for brain tumor segmentation," *Journal of Medical Imaging*, vol. 6, no. 3, p. 034002, 2019.

- [2] Z. Li, C. Wang, M. Han, Y. Xue, W. Wei, L.-J. Li, and L. Fei-Fei, "Thoracic disease identification and localization with limited supervision," in *Proceedings of the IEEE Conference on Computer Vision and Pattern Recognition*, 2018, pp. 8290–8299.
- [3] Y.-J. Huang, W. Liu, X. Wang, Q. Fang, R. Wang, Y. Wang, H. Chen, H. Chen, D. Meng, and L. Wang, "Rectifying supporting regions with mixed and active supervision for rib fracture recognition," *IEEE Transactions on Medical Imaging*, 2020.
- [4] L. Pei, L. Vidyaratne, M. M. Rahman, Z. A. Shboul, and K. M. Iftekharuddin, "Multimodal brain tumor segmentation and survival prediction using hybrid machine learning," in *International MICCAI Brainlesion Workshop*, Springer, 2019, pp. 73–81.
- [5] Z. Heng, M. Dipu, and K.-H. Yap, "Hybrid supervised deep learning for ethnicity classification using face images," in *2018 IEEE International Symposium on Circuits and Systems (ISCAS)*, IEEE, 2018, pp. 1–5.
- [6] T. Robert, N. Thome, and M. Cord, "Hybridnet: Classification and reconstruction cooperation for semi-supervised learning," in *Proceedings of the European Conference on Computer Vision (ECCV)*, 2018, pp. 153–169.
- [7] X. He and R. S. Zemel, "Learning hybrid models for image annotation with partially labeled data," in *Advances in Neural Information Processing Systems*, 2009, pp. 625–632.
- [8] M. P. Shah, S. Merchant, and S. P. Awate, "Ms-net: Mixed-supervision fully-convolutional networks for full-resolution segmentation," in *International Conference on Medical Image Computing and Computer-Assisted Intervention*, Springer, 2018, pp. 379–387.
- [9] Y. Bhalgat, M. Shah, and S. Awate, "Annotation-cost minimization for medical image segmentation using suggestive mixed supervision fully convolutional networks," *arXiv preprint arXiv:1812.11302*, 2018.
- [10] U. Upadhyay and S. P. Awate, "A mixed-supervision multilevel gan framework for image quality enhancement," in *International Conference on Medical Image Computing and Computer-Assisted Intervention*, Springer, 2019, pp. 556–564.
- [11] J. Zhang, K. Huang, J. Zhang, *et al.*, "Mixed supervised object detection with robust objectness transfer," *IEEE transactions on pattern analysis and machine intelligence*, vol. 41, no. 3, pp. 639–653, 2018.
- [12] D. Wang, M. Li, N. Ben-Shlomo, C. E. Corrales, Y. Cheng, T. Zhang, and J. Jayender, "Mixed-supervised dual-network for medical image segmentation," in *International Conference on Medical Image Computing and Computer-Assisted Intervention*, Springer, 2019, pp. 192–200.
- [13] L. Hou, D. Samaras, T. M. Kurc, Y. Gao, J. E. Davis, and J. H. Saltz, "Patch-based convolutional neural network for whole slide tissue image classification," in *Proceedings of the IEEE conference on computer vision and pattern recognition*, 2016, pp. 2424–2433.

- [14] G. Campanella, M. G. Hanna, L. Geneslaw, A. Mirafior, V. W. K. Silva, K. J. Busam, E. Brogi, V. E. Reuter, D. S. Klimstra, and T. J. Fuchs, “Clinical-grade computational pathology using weakly supervised deep learning on whole slide images,” *Nature medicine*, vol. 25, no. 8, pp. 1301–1309, 2019.
- [15] J. Li, S. Yang, X. Huang, Q. Da, X. Yang, Z. Hu, Q. Duan, C. Wang, and H. Li, “Signet ring cell detection with a semi-supervised learning framework,” in *International Conference on Information Processing in Medical Imaging*, Springer, 2019, pp. 842–854.
- [16] P. Bandi, O. Geessink, Q. Manson, M. Van Dijk, M. Balkenhol, M. Hermsen, B. E. Bejnordi, B. Lee, K. Paeng, A. Zhong, *et al.*, “From detection of individual metastases to classification of lymph node status at the patient level: The camelyon17 challenge,” *IEEE transactions on medical imaging*, vol. 38, no. 2, pp. 550–560, 2018.
- [17] X. Zhao, S. Liang, and Y. Wei, “Pseudo mask augmented object detection,” in *Proceedings of the IEEE Conference on Computer Vision and Pattern Recognition*, 2018, pp. 4061–4070.
- [18] R. Hu, P. Dollár, K. He, T. Darrell, and R. Girshick, “Learning to segment every thing,” in *Proceedings of the IEEE Conference on Computer Vision and Pattern Recognition*, 2018, pp. 4233–4241.
- [19] A. K. R. B. J. Hosang and M. H. B. Schiele, “Weakly supervised semantic labelling and instance segmentation,” *arXiv preprint arXiv:1603.07485*, 2016.
- [20] Q. Xie, E. Hovy, M.-T. Luong, and Q. V. Le, “Self-training with noisy student improves imagenet classification,” *arXiv preprint arXiv:1911.04252*, 2019.
- [21] N. Tajbakhsh, L. Jeyaseelan, Q. Li, J. N. Chiang, Z. Wu, and X. Ding, “Embracing imperfect datasets: A review of deep learning solutions for medical image segmentation,” *Medical Image Analysis*, p. 101693, 2020.
- [22] N. Tajbakhsh, B. Lai, S. P. Ananth, and X. Ding, “Errornet: Learning error representations from limited data to improve vascular segmentation,” in *2020 IEEE 17th International Symposium on Biomedical Imaging (ISBI)*, IEEE, 2020, pp. 1364–1368.
- [23] W. Wang, Q. Xia, Z. Hu, Z. Yan, Z. Li, Y. Wu, N. Huang, Y. Gao, D. Metaxas, and S. Zhang, “Few-shot learning by a cascaded framework with shape-constrained pseudo label assessment for whole heart segmentation,” *IEEE Transactions on Medical Imaging*, 2021.
- [24] C. Doersch and A. Zisserman, “Multi-task self-supervised visual learning,” in *Proceedings of the IEEE International Conference on Computer Vision*, 2017, pp. 2051–2060.
- [25] D. Terzopoulos *et al.*, “Multi-adversarial variational autoencoder networks,” in *2019 18th IEEE International Conference On Machine Learning And Applications (ICMLA)*, IEEE, 2019, pp. 777–782.
- [26] D. Nie, Y. Gao, L. Wang, and D. Shen, “Asdnet: Attention based semi-supervised deep networks for medical image segmentation,” in *International Conference on Medical Image Computing and Computer-Assisted Intervention*, Springer, 2018, pp. 370–378.
- [27] M. Jahanifar, N. A. Koohbanani, and N. Rajpoot, “Nuclick: From clicks in the nuclei to nuclear boundaries,” *arXiv preprint arXiv:1909.03253*, 2019.
- [28] L. Castrejon, K. Kundu, R. Urtasun, and S. Fidler, “Annotating object instances with a polygon-rnn,” in *Proceedings of the IEEE conference on computer vision and pattern recognition*, 2017, pp. 5230–5238.
- [29] H. Ling, J. Gao, A. Kar, W. Chen, and S. Fidler, “Fast interactive object annotation with curve-gcn,” in *Proceedings of the IEEE Conference on Computer Vision and Pattern Recognition*, 2019, pp. 5257–5266.
- [30] T. Sakinis, F. Milletari, H. Roth, P. Korfiatis, P. Kostandy, K. Philbrick, Z. Akkus, Z. Xu, D. Xu, and B. J. Erickson, “Interactive segmentation of medical images through fully convolutional neural networks,” *arXiv preprint arXiv:1903.08205*, 2019.
- [31] Z. Zhou, V. Sodha, M. M. R. Siddiquee, R. Feng, N. Tajbakhsh, M. B. Gotway, and J. Liang, “Models genesis: Generic autodidactic models for 3d medical image analysis,” in *International Conference on Medical Image Computing and Computer-Assisted Intervention*, Springer, 2019, pp. 384–393.
- [32] K. He, H. Fan, Y. Wu, S. Xie, and R. Girshick, “Momentum contrast for unsupervised visual representation learning,” *arXiv preprint arXiv:1911.05722*, 2019.
- [33] T. Chen, S. Kornblith, M. Norouzi, and G. Hinton, “A simple framework for contrastive learning of visual representations,” *arXiv preprint arXiv:2002.05709*, 2020.
- [34] O. J. Hénaff, A. Srinivas, J. De Fauw, A. Razavi, C. Doersch, S. Eslami, and A. v. d. Oord, “Data-efficient image recognition with contrastive predictive coding,” *arXiv preprint arXiv:1905.09272*, 2019.
- [35] N. Tajbakhsh, J. Y. Shin, S. R. Gurudu, R. T. Hurst, C. B. Kendall, M. B. Gotway, and J. Liang, “Convolutional neural networks for medical image analysis: Full training or fine tuning?” *IEEE transactions on medical imaging*, vol. 35, no. 5, pp. 1299–1312, 2016.
- [36] N. Tajbakhsh, Y. Hu, J. Cao, X. Yan, Y. Xiao, Y. Lu, J. Liang, D. Terzopoulos, and X. Ding, “Surrogate supervision for medical image analysis: Effective deep learning from limited quantities of labeled data,” in *2019 IEEE 16th International Symposium on Biomedical Imaging (ISBI 2019)*, IEEE, 2019, pp. 1251–1255.
- [37] J. Xu, L. Xiang, Q. Liu, H. Gilmore, J. Wu, J. Tang, and A. Madabhushi, “Stacked sparse autoencoder (ssae) for nuclei detection on breast cancer histopathology images,” *IEEE transactions on medical imaging*, vol. 35, no. 1, pp. 119–130, 2015.
- [38] J. Li, Z. Hu, and S. Yang, “Accurate nuclear segmentation with center vector encoding,” in *International Conference on Information Processing in Medical Imaging*, Springer, 2019, pp. 394–404.
- [39] Y. Zhou, O. F. Onder, Q. Dou, E. Tsougenis, H. Chen, and P.-A. Heng, “Cia-net: Robust nuclei instance segmentation with contour-aware information aggregation,”

- in *International Conference on Information Processing in Medical Imaging*, Springer, 2019, pp. 682–693.
- [40] H. Chen, X. Qi, L. Yu, and P.-A. Heng, “Dcan: Deep contour-aware networks for accurate gland segmentation,” in *Proceedings of the IEEE conference on Computer Vision and Pattern Recognition*, 2016, pp. 2487–2496.
- [41] N. Coudray, P. S. Ocampo, T. Sakellaropoulos, N. Narula, M. Snuderl, D. Fenyö, A. L. Moreira, N. Razavian, and A. Tsirigos, “Classification and mutation prediction from non-small cell lung cancer histopathology images using deep learning,” *Nature medicine*, vol. 24, no. 10, pp. 1559–1567, 2018.
- [42] J. Cheng, J. Zhang, Y. Han, X. Wang, X. Ye, Y. Meng, A. Parwani, Z. Han, Q. Feng, and K. Huang, “Integrative analysis of histopathological images and genomic data predicts clear cell renal cell carcinoma prognosis,” *Cancer research*, vol. 77, no. 21, e91–e100, 2017.
- [43] W. Shao, Z. Han, J. Cheng, L. Cheng, T. Wang, L. Sun, Z. Lu, J. Zhang, D. Zhang, and K. Huang, “Integrative analysis of pathological images and multi-dimensional genomic data for early-stage cancer prognosis,” *IEEE Transactions on Medical Imaging*, vol. 39, no. 1, pp. 99–110, 2019.
- [44] X. Zhan, J. Cheng, Z. Huang, Z. Han, B. Helm, X. Liu, J. Zhang, T.-F. Wang, D. Ni, and K. Huang, “Correlation analysis of histopathology and proteogenomics data for breast cancer,” *Molecular & Cellular Proteomics*, vol. 18, no. 8 suppl 1, S37–S51, 2019.
- [45] Q. Wang, Q. Shen, Z. Zhang, C. Cai, H. Lu, X. Zhou, and J. Xu, “Prediction of gene mutation in lung cancer based on deep learning and histomorphology analysis,” *Sheng wu yi xue gong cheng xue za zhi= Journal of biomedical engineering= Shengwu yixue gongchengxue zazhi*, vol. 37, no. 1, pp. 10–18, 2020.
- [46] Z. Swiderska-Chadaj, H. Pinckaers, M. van Rijthoven, M. Balkenhol, M. Melnikova, O. Geessink, Q. Manson, M. Sherman, A. Polonia, J. Parry, *et al.*, “Learning to detect lymphocytes in immunohistochemistry with deep learning,” *Medical image analysis*, vol. 58, p. 101 547, 2019.
- [47] A. Basavanahally, J. Xu, A. Madabhushi, and S. Ganesan, “Computer-aided prognosis of er+ breast cancer histopathology and correlating survival outcome with oncotype dx assay,” in *2009 IEEE International Symposium on Biomedical Imaging: From Nano to Macro*, IEEE, 2009, pp. 851–854.
- [48] X. Zhang, T. C. Cornish, L. Yang, T. D. Bennett, D. Ghosh, and F. Xing, “Generative adversarial domain adaptation for nucleus quantification in images of tissue immunohistochemically stained for ki-67,” *JCO Clinical Cancer Informatics*, vol. 4, pp. 666–679, 2020.
- [49] A. Madabhushi, M. Khorrani, and V. Velcheti, *Predicting disease recurrence following trimodality therapy in non-small cell lung cancer using computed tomography derived radiomic features and clinico-pathologic features*, US Patent 10,441,225, Oct. 2019.
- [50] M. Shaban, R. Awan, M. M. Fraz, A. Azam, D. Snead, and N. M. Rajpoot, “Context-aware convolutional neural network for grading of colorectal cancer histology images,” *arXiv preprint arXiv:1907.09478*, 2019.
- [51] P. Ström, K. Kartasalo, H. Olsson, L. Solorzano, B. Delahunt, D. M. Berney, D. G. Bostwick, A. J. Evans, D. J. Grignon, P. A. Humphrey, *et al.*, “Pathologist-level grading of prostate biopsies with artificial intelligence,” *arXiv preprint arXiv:1907.01368*, 2019.
- [52] K. Nagpal, D. Foote, Y. Liu, P.-H. C. Chen, E. Wulczyn, F. Tan, N. Olson, J. L. Smith, A. Mohtashamian, J. H. Wren, *et al.*, “Development and validation of a deep learning algorithm for improving gleason scoring of prostate cancer,” *NPJ digital medicine*, vol. 2, no. 1, pp. 1–10, 2019.
- [53] M. Khened, A. Kori, H. Rajkumar, B. Srinivasan, and G. Krishnamurthi, “A generalized deep learning framework for whole-slide image segmentation and analysis,” *arXiv preprint arXiv:2001.00258*, 2020.
- [54] M. Y. Lu, R. J. Chen, J. Wang, D. Dillon, and F. Mahmood, “Semi-supervised histology classification using deep multiple instance learning and contrastive predictive coding,” *arXiv preprint arXiv:1910.10825*, 2019.
- [55] K. Tomczak, P. Czerwińska, and M. Wiznerowicz, “The cancer genome atlas (tcga): An immeasurable source of knowledge,” *Contemporary oncology*, vol. 19, no. 1A, A68, 2015.
- [56] S. Takahama, Y. Kurose, Y. Mukuta, H. Abe, M. Fukayama, A. Yoshizawa, M. Kitagawa, and T. Harada, “Multi-stage pathological image classification using semantic segmentation,” in *Proceedings of the IEEE International Conference on Computer Vision*, 2019, pp. 10 702–10 711.
- [57] Y. Zhou, S. Graham, N. Alemi Koohbanani, M. Shaban, P.-A. Heng, and N. Rajpoot, “Cgc-net: Cell graph convolutional network for grading of colorectal cancer histology images,” in *Proceedings of the IEEE International Conference on Computer Vision Workshops*, 2019, pp. 0–0.
- [58] J. Li, Y. Wong, Q. Zhao, and M. S. Kankanhalli, “Learning to learn from noisy labeled data,” in *Proceedings of the IEEE/CVF Conference on Computer Vision and Pattern Recognition*, 2019, pp. 5051–5059.
- [59] A. Paszke, S. Gross, S. Chintala, G. Chanan, E. Yang, Z. DeVito, Z. Lin, A. Desmaison, L. Antiga, and A. Lerer, “Automatic differentiation in pytorch,” in *NIPS-W*, 2017.
- [60] A. Goode, B. Gilbert, J. Harkes, D. Jukic, and M. Satyanarayanan, “Openslide: A vendor-neutral software foundation for digital pathology,” *Journal of pathology informatics*, vol. 4, 2013.
- [61] N. Otsu, “A threshold selection method from gray-level histograms,” *IEEE transactions on systems, man, and cybernetics*, vol. 9, no. 1, pp. 62–66, 1979.
- [62] F. Yu, D. Wang, E. Shelhamer, and T. Darrell, “Deep layer aggregation,” in *Proceedings of the IEEE Conference on Computer Vision and Pattern Recognition*, 2018, pp. 2403–2412.